Vehicle System Dynamics

ISSN: 0042-3114 (Print) 1744-5159 (Online) Journal homepage: https://www.tandfonline.com/loi/nvsd20

Dual extended Kalman filter for vehicle state and parameter estimation

T. A. Wenzel, K. J. Burnham, M. V. Blundell & R. A. Williams

To cite this article: T. A. Wenzel, K. J. Burnham, M. V. Blundell & R. A. Williams (2006) Dual extended Kalman filter for vehicle state and parameter estimation, Vehicle System Dynamics, 44:2, 153-171, DOI: 10.1080/00423110500385949

To link to this article: https://doi.org/10.1080/00423110500385949

Vehicle System Dynamics
Vol. 44, No. 2, February 2006, 153–171

Taylor & Francis
Taylor & Francis Group

Dual extended Kalman filter for vehicle state and parameter estimation

T. A. WENZEL*†, K. J. BURNHAM†, M. V. BLUNDELL† and R. A. WILLIAMS‡

†Control Theory and Applications Centre, Coventry University, Priory Street, CV1 5FB, Coventry, UK
‡Jaguar and Land Rover Research, Whitley, UK

The article demonstrates the implementation of a model-based vehicle estimator, which can be used for combined estimation of vehicle states and parameters. The estimator is realised using the dual extended Kalman filter (DEKF) technique, which makes use of two Kalman filters running in parallel, thus 'splitting' the state and parameter estimation problems. Note that the two problems cannot be entirely separated due to their inherent interdependencies. This technique provides several advantages, such as the possibility to switch off the parameter estimator, once a sufficiently good set of estimates has been obtained. The estimator is based on a four-wheel vehicle model with four degrees of freedom, which accommodates the dominant modes only, and is designed to make use of several interchangeable tyre models. The paper demonstrates the appropriateness of the DEKF. Results to date indicate that this is an effective approach, which is considered to be of potential benefit to the automotive industry.

Keywords: Vehicle dynamics control; Dual extended Kalman filter; State and parameter estimation; Modelling and simulation technology

1. Introduction

The automotive industry has made significant technological progress over the last decade or so concerning active vehicle stability control, and hence improved safety, by developing and introducing microprocessor control systems. Among these controllers are systems such as the anti-lock braking system, active roll control, active front steering and electronic stability programs [1]. Effective operation of each of these systems depends on an accurate knowledge of the vehicle states, such as velocity, lateral acceleration, yaw rate, as well as vehicle and tyre side slip. Due to physical and economic reasons, only a few of these states can actually be obtained by measurement, thus the knowledge of the majority of these states is required to be obtained by online estimation. As the control systems currently operate independently, their functions are based on their individual vehicle state estimations. For a vehicle manufacturer, it may be more desirable to develop a coordinated approach, overseeing these control systems by designing a single state estimator, which is common to all systems, and hierarchically configured to provide the necessary states.

*Corresponding author. Tel.: +44-2476-888972; Email: t.wenzel@coventry.ac.uk/ctac@coventry.ac.uk

Vehicle System Dynamics
ISSN 0042-3114 print/ISSN 1744-5159 online © 2006 Taylor & Francis
http://www.tandf.co.uk/journals
DOI: 10.1080/00423110500385949

Accurate knowledge of vehicle states is essential and, not surprisingly, there are different approaches for their estimation. However, most of these approaches are not without their restrictions and limitations. Many of the estimators work only with a reduced number of states or a reduced vehicle model, such as a bicycle model. Approaches can be found that use this model for the estimation of side slip angle and yaw rate [2] or for lateral acceleration, yaw rate and tyre slip angles [3, 4].

Other approaches make use of more comprehensive vehicle models, such as a four-wheel model. For example, in ref. [5], use is made of a four-wheel model to estimate lateral velocity and yaw rate, as well as the vehicle's roll motion, but it has the drawback that the implemented estimator requires the use of a whole set of additional costly acceleration sensors. A four-wheel model is also used by Huh *et al.* [6] to estimate longitudinal and lateral velocity and yaw and roll motion.

All the above approaches have another common limitation. They use fixed vehicle parameters, such as mass, moments of inertia and/or position of the centre of gravity (cog), which are assumed to be known. While approximate values for these parameters are known, such as the weight of an empty vehicle, these parameters may vary significantly from one journey to the next. For example, when comparing a vehicle occupied only by the driver with a vehicle with passengers, additional luggage and a full fuel tank, then the mass could easily vary by several hundred kilograms. There are approaches to estimate some of the parameters, such as mass [7], but these depend on the existence of further measured states. It can be shown that appropriate knowledge of these vehicle parameters is of importance for effective estimation of the various vehicle states. Recognising the need for such knowledge, the estimator described in this paper additionally estimates the parameters to achieve an improved estimation of the vehicle states.

2. Vehicle model

The state and parameter estimator presented here is based on a four-wheel vehicle model, which comprises four degrees of freedom: the motion in the longitudinal direction x, *i.e.* the longitudinal velocity v_x; the motion in the lateral direction y or lateral velocity v_y; yaw around the vertical axis z, described by the yaw rate $\dot{\psi}$ and roll with regard to the longitudinal axis x, *i.e.* the roll angle ϕ.

Other states that depend directly on these four states can be directly derived, such as longitudinal and lateral accelerations a_x and a_y, or depend indirectly on these states, such as body slip angle β and torque Γ around the z-axis. The tyre states, such as wheel slip angle α_{ij} and slip rate s_{ij}, as well as the wheel forward velocities v_{ij} and rotational velocities ω_{ij} are also of importance. Note that for the states concerning the tyres, the indices ij represent the tyre location on the vehicle, where i indicates the front (f) or rear (r) tyre and j indicates the left (l) or right (r) side.

The vehicle states are largely dependent on the key operating parameters of a vehicle. Of particular importance here are the vehicle mass m, moments of inertia J_z and J_{sx} and the distances b and c between the centre of gravity and the front and rear axles, respectively. Figure 1 illustrates the main states and parameters for a vehicle.

The interrelationships between the different vehicle dynamic states can be described by differential equations. Various approaches for formulating these equations can be found in the standard literature. The vehicle model implemented here utilises standard formulae, which can be obtained from refs. [8, 9]. The differential equations for the calculation of longitudinal

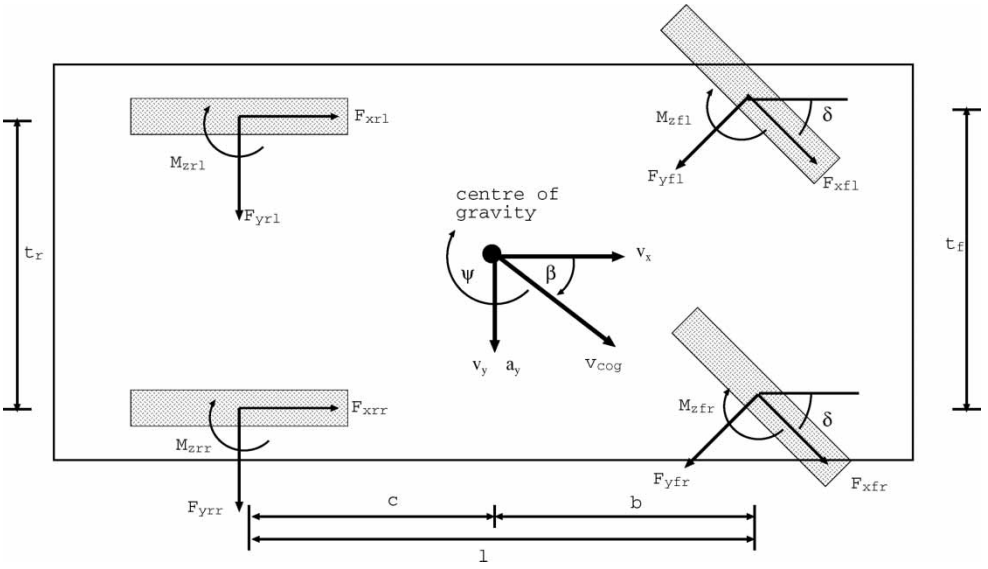

Figure 1. Illustration of vehicle states and parameters.

and lateral acceleration are as follows:

$$a_x = \frac{1}{m}(F_{x\mathrm{fl}}\cos\delta - F_{y\mathrm{fl}}\sin\delta + F_{x\mathrm{fr}}\cos\delta - F_{y\mathrm{fr}}\sin\delta + F_{x\mathrm{rl}} + F_{x\mathrm{rr}}) \tag{1}$$

$$a_y = \frac{1}{m}(F_{y\mathrm{fl}}\cos\delta + F_{x\mathrm{fl}}\sin\delta + F_{y\mathrm{fr}}\cos\delta + F_{x\mathrm{fr}}\sin\delta + F_{y\mathrm{rl}} + F_{y\mathrm{rr}}) \tag{2}$$

$$\dot{v}_x = a_x + v_y\dot{\psi} \tag{3}$$

$$\dot{v}_y = a_y - v_x\dot{\psi} \tag{4}$$

Yaw and roll motion can be obtained from:

$$\ddot{\psi} = \frac{\Gamma}{J_z} \tag{5}$$

$$\Gamma = \frac{t_\mathrm{f}}{2}F'_{x\mathrm{fl}} - \frac{t_\mathrm{f}}{2}F'_{x\mathrm{fr}} + \frac{t_\mathrm{r}}{2}F_{x\mathrm{rl}} - \frac{t_\mathrm{r}}{2}F_{x\mathrm{rr}} + bF'_{y\mathrm{fl}} + bF'_{y\mathrm{fr}} - cF_{y\mathrm{rl}} - cF_{y\mathrm{rr}} + M_{z\mathrm{fl}} + M_{z\mathrm{fr}} + M_{z\mathrm{rl}} + M_{z\mathrm{rr}} \tag{6}$$

$$\ddot{\phi} = \frac{1}{J_{sx}}\left(-m_s h_s a_y + \phi(m_s g h_s - \kappa_\phi) - \dot{\phi}\beta_\phi\right) \tag{7}$$

where the F's denote the tyre forces acting in the vehicle coordinate system as follows:

$$F'_{xij} = F_{xij}\cos\delta - F_{yij}\sin\delta \tag{8}$$

$$F'_{yij} = F_{yij}\cos\delta + F_{xij}\sin\delta \tag{9}$$

with t_f and t_r denoting the front and rear track widths, respectively. For the roll motion only the sprung mass is taken into account, where m_s denotes the sprung mass, J_sx the moment of inertia around the longitudinal axis and h_s denotes the height of the cog. The constants κ_ϕ and β_ϕ denote the roll stiffness and roll damping, respectively.

The longitudinal and lateral velocities, the steer angle of the front wheels and the yaw rate are then used as a basis for the calculation of the tyre slip angles α_{ij} as well as the vehicle body slip angle β:

$$\alpha_\mathrm{fl,fr} = \delta - \arctan\left(\frac{v_y + b\dot{\psi}}{v_x \pm t_\mathrm{f}\dot{\psi}/2}\right) \tag{10}$$

$$\alpha_\mathrm{rl,rr} = \arctan\left(\frac{-v_y + c\dot{\psi}}{v_x \pm t_\mathrm{r}\dot{\psi}/2}\right) \tag{11}$$

$$\beta = \arctan\left(\frac{v_y}{v_x}\right) \tag{12}$$

The slip rates of the tyres are calculated based on the ratio between the rotational wheel velocities ω_{ij} and the actual velocities v_{ij} of the wheel centres on the road, following the approach in ref. [10]:

$$s_{ij} = \frac{\omega_{ij} r}{v_{ij}} - 1 \tag{13}$$

where

$$v_\mathrm{fl,fr} = v_\mathrm{cog} + \dot{\psi}\left(\pm\frac{t_\mathrm{f}}{2} - b\beta\right) \tag{14}$$

$$v_\mathrm{rl,rr} = v_\mathrm{cog} + \dot{\psi}\left(\pm\frac{t_\mathrm{r}}{2} + c\beta\right) \tag{15}$$

in which v_cog denotes the absolute velocity of the cog.

Due to longitudinal and lateral acceleration of the vehicle, the load distribution can vary significantly during a journey. The load distribution can be expressed by the vertical forces that act on each of the four wheels. These can be calculated as follows:

$$F_{z\mathrm{fl},z\mathrm{fr}} = \left(\frac{1}{2}mg \pm m\frac{a_y h}{t_\mathrm{f}}\right)\frac{c}{\ell} - \frac{1}{2}ma_x\frac{h}{\ell} \tag{16}$$

$$F_{z\mathrm{rl},z\mathrm{rr}} = \left(\frac{1}{2}mg \pm m\frac{a_y h}{t_\mathrm{r}}\right)\frac{b}{\ell} + \frac{1}{2}ma_x\frac{h}{\ell} \tag{17}$$

The lateral acceleration used in equations (16) and (17) is that which occurs at the cog. It should be noted that, in general, this cannot be measured, because an accelerometer cannot normally be placed in the exact cog, due to design constrictions. Also, the position of the cog will vary depending on the actual load distribution of the vehicle. Consequently, the measured and the actual acceleration will differ due to yaw and roll movement, depending on the actual sensor position. A simplified approach for compensating for this discrepancy can be found in ref. [11], which accommodates the additional acceleration measurement due to both gravitational acceleration g and yaw acceleration $\ddot{\psi}$:

$$a_{y,\mathrm{sensor}} = (a_y + \ddot{\psi}x_a)\cos\phi + g\sin\phi \tag{18}$$

where x_a is the longitudinal distance between the accelerometer and the cog. However, not only the roll angle ϕ, but also the effects of roll rate $\dot{\phi}$ and roll acceleration $\ddot{\phi}$ as well as

yaw rate are required to be considered. Taking into account the accelerometer position with a height h_z above the roll axis, the longitudinal distance x_a and lateral distance y_a from the cog and making use of the basic kinematic equations, which may be found in ref. [12], a refined expression (superceding equation (18)) for the measured lateral acceleration can be deduced:

$$a_{y,\text{sensor}} = \left(a_y + \ddot{\psi} x_a - \dot{\psi}^2 y_a + \ddot{\phi} h_z - \dot{\phi}^2 y_a\right) \cdot \cos\phi + g \sin\phi \tag{19}$$

This can be simplified by using the approximations $\sin\phi \approx \phi$ and $\cos\phi \approx 1$ for small angles of ϕ. Furthermore, assuming a lateral position of the accelerometer over the vehicle's centre line along the x-axis, and defining the longitudinal position of the accelerometer as b_a behind the front axle, equation (19) can be simplified to:

$$a_{y,\text{sensor}} = \left(a_y + \ddot{\psi}(b - b_a) + \ddot{\phi} h_z\right) + g\phi \tag{20}$$

3. Tyre model

The whole motion of the vehicle is a direct result of the forces (neglecting the aerodynamic forces) that are generated between the road and the four tyres. The dynamic equations outlined above show that all states depend on the calculation of the vehicle accelerations, which in turn depend very much on accurate knowledge of the tyre forces, as can be seen in equations (1), (2) and (6). Because the actual tyre forces cannot be measured, they need to be calculated based on the estimated and measured states.

There are different approaches for achieving this, such as the so-called 'Magic Formula' by Pacejka [13], the tyre model by Fiala [14] or the 'TMeasy' tyre model [15]. The estimator described in this article is configured such that use may be made of any suitable tyre model, thus facilitating comparison between the various approaches.

Essentially, the tyre models differ in terms of their relative complexities, *i.e.* number of coefficients, which are specific for each particular model. The number of coefficients can vary widely, *e.g.* from 9 in the Fiala model to 82 in the latest version of the Magic Formula. These parameters are normally obtained by extensive experimental testing of tyres on a test rig.

The tyre models require certain common inputs, such as tyre slip angle, tyre slip rates and vertical forces acting on each tyre. The example presented in section 5 makes use of both the Magic Formula and TMeasy for determining the tyre forces. The Magic Formula is used to calculate the longitudinal and lateral tyre forces F_x and F_y as well as the self-aligning moments M_z by a scheme, which is given by the following equations [16]:

$$y = D \sin[C \arctan\{Bx - E(Bx - \arctan Bx)\}] \tag{21}$$

$$Y(X) = y(x) + S_v \tag{22}$$

$$x = X + S_h \tag{23}$$

where the general output variable Y in equation (22) is used to represent the tyre forces F_x and F_y and self-aligning moments M_z, while the input variable X is used to represent tyre slip rate s (when calculating F_x) or tyre slip angle α (when calculating F_y and M_z). The main issue is then the determination of the coefficients B, C, D, E, S_v and S_h, which are calculated using the vertical tyre force F_z, the road friction μ and the specific tyre model parameters. Note that y and x in equations (21)–(23) are merely intermediate variables in determining the general output $Y(X)$.

In contrast to this approach, which calculates each directional force separately, the TMeasy tyre model calculates the resulting force F on the tyre by a combination of rational and

polynomial functions, as can be found in ref. [15]. Using the same notation as in ref. [15], the force on the tyre as a function of slip is given by:

$$F(s) = \begin{cases} s^M dF^0 \frac{\sigma}{1+\sigma(\sigma+dF^0(s^M/F^M)-2)}, & \sigma = \dfrac{s}{s^M}, \quad 0 \le s \le s^M \\ F^M - (F^M - F^G)\sigma^2(3-2\sigma), & \sigma = \dfrac{s-s^M}{s^G - s^M}, \quad s^M < s \le s^G \\ F^G, & s > s^G \end{cases} \tag{24}$$

where s denotes the resulting slip. The maximal possible resulting force is denoted by F^M and the resulting force in full sliding condition is denoted by F^G. The corresponding slip rates are denoted by s^M and s^G, respectively. The actual values for the forces F^M and F^G and the slip rates s^M and s^G are obtained by performing quadratic interpolation, depending on the vertical force, using values specified in look-up tables. Furthermore, dF^0 denotes the overall initial inclination of the horizontal tyre forces. The resulting force F may be decomposed into longitudinal and lateral forces:

$$F_x = F\cos\alpha \tag{25}$$

$$F_y = F\sin\alpha \tag{26}$$

Despite the complexity of the tyre models, there are several reasons why such models do not match the actual tyre forces perfectly [17]. For example, the rig testing may have taken place under well behaved conditions corresponding to operation in a linear region, while the tyres may find themselves in rapidly changing conditions and may even experience effects of non-linear behaviour at the limit of the linear region. In addition, although representative surfaces may be used for testing, these surfaces can differ significantly from the road surface on which the tyres are subsequently used. Thus, when choosing and using a tyre model, due care needs to be given, recognising that whilst a model may be quite advanced, it will nevertheless introduce an element of uncertainty into the overall vehicle model.

4. Dual extended Kalman filter

The state and parameter estimator proposed in this article is based on the Kalman filtering technique, which is a widely used conceptual two-stage prediction/correction approach that has found application in a variety of areas. Whilst the Kalman filter (KF) was originally proposed by Kalman [18] for the estimation of the non-measurable states in linear systems, it has found wide usage in its extended form for state estimation of non-linear systems as well as joint state/parameter estimation for linear and non-linear systems. The fundamental operation of the KF is a successive process of prediction based on system input, followed by the correction based on measurable system output.

A powerful extension, developed for state estimation in non-linear systems, is the so-called extended Kalman filter (EKF), in which the state equations are linearised at each working point [19]. The main concept is the same as the standard KF, but the computational complexity is enlarged, as the linearisation requires the evaluation of a Jacobian matrix at each time step. Recognising that the resulting augmented system is in fact non-linear, such an approach has also been developed for joint state/parameter estimation for linear systems.

A further development also designed for state and parameter estimation is the dual extended Kalman filter (DEKF), which was proposed by Wan and Nelson [20]. This variant provides a 'boot-strapping' procedure for combined state and parameter estimation using two EKFs in

parallel. Figure 2 illustrates the working scheme of the DEKF, consisting of alternating steps of prediction followed by correction.

The vehicle parameters, such as mass, can be assumed to be constant during a journey or vary at least only marginally, *e.g.* small reduction due to consumption of fuel. This indicates an advantage of using two EKFs instead of a single EKF, which combines both state and parameter vectors. Using the DEKF, it is possible to switch off the parameter estimator, once a sufficiently good set of estimates for the parameters have been found. This should increase the performance of the state estimator, as it reduces the parameter uncertainties as well as disturbances arising from the varying model parameters.

In general a non-linear system can be formulated as:

$$\mathbf{x}_{\mathrm{s}}(t+1) = f(\mathbf{x}_{\mathrm{s}}(t), \mathbf{u}(t), \mathbf{x}_{\mathrm{p}}(t), \mathbf{w}(t)) \tag{27a}$$

$$\mathbf{y}(t) = h(\mathbf{x}_{\mathrm{s}}(t), \mathbf{v}(t), \mathbf{x}_{\mathrm{p}}(t)) \tag{27b}$$

where $\mathbf{x}_{\mathrm{s}}$ is the state vector, $\mathbf{x}_{\mathrm{p}}$ is the parameter vector, $\mathbf{u}$ is the input vector, $\mathbf{y}$ is the output vector, with $\mathbf{w}$ and $\mathbf{v}$ being the process noise and output noise vectors respectively. The basic equations for the DEKF for such a non-linear system can be found in [20]; they are stated here as follows:

Parameter prediction:

$$\hat{\mathbf{x}}_{\mathrm{p}}^{-}(t) = \hat{\mathbf{x}}_{\mathrm{p}}(t-1) \tag{28}$$

$$\mathbf{\Phi}_{\mathrm{p}}^{-}(t) = \mathbf{\Phi}_{\mathrm{p}}^{-}(t-1) + \mathbf{R}_{\mathrm{p}} \tag{29}$$

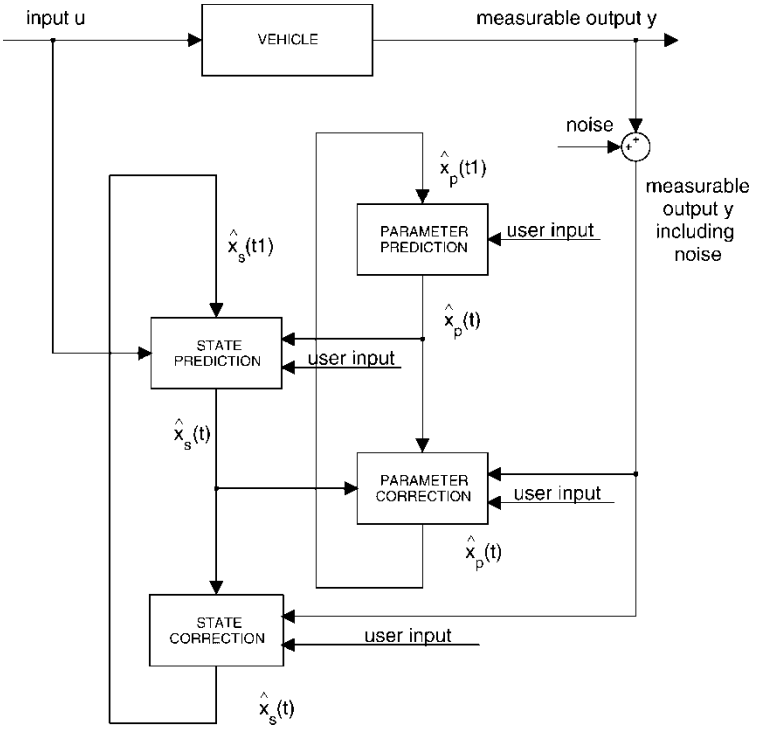

Figure 2. Scheme of DEKF.

State prediction:

$$\hat{\mathbf{x}}_{\mathrm{s}}^{-}(t) = f(\hat{\mathbf{x}}_{\mathrm{s}}^{-}(t-1), \mathbf{u}(t), \hat{\mathbf{x}}_{\mathrm{p}}^{-}(t)) \tag{30}$$

$$\mathbf{\Phi}_{\mathrm{s}}^{-}(t) = \mathbf{J}_{\mathrm{s}}(t)\mathbf{\Phi}_{\mathrm{s}}^{-}(t-1)\mathbf{J}_{\mathrm{s}}^{\mathrm{T}}(t) + \mathbf{R}_{\mathrm{s}} \tag{31}$$

State correction:

$$\mathbf{K}_{\mathrm{s}}(t) = \mathbf{\Phi}_{\mathrm{s}}^{-}(t)\mathbf{H}_{\mathrm{s}}^{\mathrm{T}}[\boldsymbol{\sigma}_{\mathrm{s}} + \mathbf{H}_{\mathrm{s}}\mathbf{\Phi}_{\mathrm{s}}^{-}(t)\mathbf{H}_{\mathrm{s}}^{\mathrm{T}}]^{-1} \tag{32}$$

$$\hat{\mathbf{x}}_{\mathrm{s}}(t) = \hat{\mathbf{x}}_{\mathrm{s}}^{-}(t) + \mathbf{K}_{\mathrm{s}}(t)[\mathbf{y}(t) - \mathbf{H}_{\mathrm{s}}\hat{\mathbf{x}}_{\mathrm{s}}^{-}(t)] \tag{33}$$

$$\mathbf{\Phi}_{\mathrm{s}}(t) = [\mathbf{I} - \mathbf{K}_{\mathrm{s}}(t)\mathbf{H}_{\mathrm{s}}]\mathbf{\Phi}_{\mathrm{s}}^{-}(t) \tag{34}$$

Parameter correction:

$$\mathbf{K}_{\mathrm{p}}(t) = \mathbf{\Phi}_{\mathrm{p}}^{-}(t)\mathbf{H}_{\mathrm{p}}^{\mathrm{T}}[\boldsymbol{\sigma}_{\mathrm{p}} + \mathbf{H}_{\mathrm{p}}\mathbf{\Phi}_{\mathrm{p}}^{-}(t)\mathbf{H}_{\mathrm{p}}^{\mathrm{T}}]^{-1} \tag{35}$$

$$\hat{\mathbf{x}}_{\mathrm{p}}(t) = \hat{\mathbf{x}}_{\mathrm{p}}^{-}(t) + \mathbf{K}_{\mathrm{p}}(t)[\mathbf{y}(t) - \mathbf{H}_{\mathrm{s}}\hat{\mathbf{x}}_{\mathrm{s}}^{-}(t)] \tag{36}$$

$$\mathbf{\Phi}_{\mathrm{p}}(t) = [\mathbf{I} - \mathbf{K}_{\mathrm{p}}(t)\mathbf{H}_{\mathrm{p}}]\mathbf{\Phi}_{\mathrm{p}}^{-}(t) \tag{37}$$

Here, $\mathbf{R}_{\mathrm{s}}$ and $\mathbf{R}_{\mathrm{p}}$ are user-specified process noise covariance matrices for the state and parameter estimators, respectively; $\boldsymbol{\sigma}_{\mathrm{s}}$ and $\boldsymbol{\sigma}_{\mathrm{p}}$ are the corresponding output noise covariance matrices, respectively, and $\mathbf{\Phi}_{\mathrm{s}}$ and $\mathbf{\Phi}_{\mathrm{p}}$ are the covariance matrices of the estimation errors, respectively.

Using equations (1)–(20) for defining the system dynamic equations $f(\cdot)$ and $h(\cdot)$, the Jacobian matrices $\mathbf{J}_{\mathrm{s}}$ and $\mathbf{H}_{\mathrm{s}}$ for the state and output equations are then given, respectively, by:

$$\mathbf{J}_{\mathrm{s}} = \begin{bmatrix} \dfrac{\partial f_1}{\partial x_1} & \cdots & \dfrac{\partial f_1}{\partial x_m} \\ \vdots & & \vdots \\ \dfrac{\partial f_m}{\partial x_1} & \cdots & \dfrac{\partial f_m}{\partial x_m} \end{bmatrix} \tag{38}$$

$$\mathbf{H}_{\mathrm{s}} = \begin{bmatrix} 0 & 0 & 1 & 0 & \cdots & 0 \\ 0 & 0 & 0 & 0 & \cdots & 1 \\ 1 & 0 & 0 & 0 & \cdots & 0 \end{bmatrix} \tag{39}$$

The input vector $\mathbf{u}$ and the output vector $\mathbf{y}$ consist of the available measurable vehicle states:

$$\mathbf{u} = \begin{bmatrix} \delta \\ \omega_{\mathrm{fl}} \\ \omega_{\mathrm{fr}} \\ \omega_{\mathrm{rl}} \\ \omega_{\mathrm{rr}} \end{bmatrix} \tag{40}$$

$$\mathbf{y} = \begin{bmatrix} \dot{\psi} \\ a_{y,\mathrm{sensor}} \\ v_x \end{bmatrix} = \mathbf{H}_{\mathrm{s}}\mathbf{x}_{\mathrm{s}} \tag{41}$$

The state and parameter vectors comprise the internal states required by the dynamic safety control systems and the unknown vehicle parameters, respectively:

$$\mathbf{x}_\mathrm{s} = [v_x\ v_y\ \dot{\psi}\ a_y\ \Gamma\ \beta\ a_x\ \alpha_\mathrm{fl}\ \alpha_\mathrm{fr}\ \alpha_\mathrm{rl}\ \alpha_\mathrm{rr}\ F_{z,\mathrm{fl}}\ F_{z,\mathrm{fr}}\ F_{z,\mathrm{rl}}\ F_{z,\mathrm{rr}}\ s_\mathrm{fl}\ s_\mathrm{fr}\ s_\mathrm{rl}\ s_\mathrm{rr}\ \phi\ \dot{\phi}\ a_{y,\mathrm{sensor}}]^\mathrm{T} \tag{42}$$

$$\mathbf{x}_\mathrm{p} = \begin{bmatrix} m \\ J_z \\ b \end{bmatrix} \tag{43}$$

Note that the matrix $\mathbf{H}_\mathrm{p}$ is required, which can be simplified as follows [21]:

$$\mathbf{H}_\mathrm{p} = \mathbf{H}_\mathrm{s} \frac{\partial f(\hat{\mathbf{x}}_\mathrm{s}, \hat{\mathbf{x}}_\mathrm{p})}{\partial \hat{\mathbf{x}}_\mathrm{p}} \tag{44}$$

$$= \begin{bmatrix} \dfrac{\partial \dot{\psi}}{\partial m} & \dfrac{\partial \dot{\psi}}{\partial J_z} & \dfrac{\partial \dot{\psi}}{\partial b} \\ \dfrac{\partial a_{y,\mathrm{sensor}}}{\partial m} & \dfrac{\partial a_{y,\mathrm{sensor}}}{\partial J_z} & \dfrac{\partial a_{y,\mathrm{sensor}}}{\partial b} \\ \dfrac{\partial v_x}{\partial m} & \dfrac{\partial v_x}{\partial J_z} & \dfrac{\partial v_x}{\partial b} \end{bmatrix} \tag{45}$$

Equations (28)–(37) depend on the definition of the four covariance matrices. Since for both parallel estimators, the same output $\mathbf{y}$ is used, the measurement noise covariances are the same: $\boldsymbol{\sigma}_\mathrm{s} = \boldsymbol{\sigma}_\mathrm{p}$, denoted $\boldsymbol{\sigma}$. Thus the number of covariance matrices is reduced to three.

According to ref. [22], the measurement noise covariance matrix $\boldsymbol{\sigma}$ can be obtained via off-line sample measurements, while it is more difficult to define the process noise covariance matrix. In the case of state estimation, the estimator works well with a fairly 'crude' initial setting, such as setting the process noise covariance matrix to the identity matrix with the same constant value R_0 for the diagonal elements. Experiments show that setting R_0 to a sufficiently large value, such as $R_0 = 10{,}000$, results in good state estimates. In this example, good results for the state estimation were obtained with the following settings:

$$\boldsymbol{\sigma}_\mathrm{s} = \boldsymbol{\sigma}_\mathrm{p} = \begin{bmatrix} s_{\dot{\psi}}^2 & 0 & 0 \\ 0 & s_{a_{y,\mathrm{sensor}}}^2 & 0 \\ 0 & 0 & s_{v_x}^2 \end{bmatrix} \tag{46}$$

$$\mathbf{R}_\mathrm{s} = R_0 \mathbf{I} \tag{47}$$

However, the parameter estimation is found to be more sensitive to the actual process noise covariance matrix settings. The initial covariance matrix for the parameter estimator was set to the following diagonal matrix:

$$\mathbf{R}_\mathrm{p} = \begin{bmatrix} s_m^2 & 0 & 0 \\ 0 & s_{J_z}^2 & 0 \\ 0 & 0 & s_b^2 \end{bmatrix} \tag{48}$$

For the following example the process noise covariance matrix $\mathbf{R}_\mathrm{p}$ was set such that the variables s_m, s_{J_z} and s_b were of an order of approximately 1% of the corresponding actual values for the parameters m, J_z and b.

The better the parameter estimation becomes, the smaller become the model uncertainties. This can be taken into account by weighting the covariance matrices exponentially. Thus, in a similar manner as in ref. [23], the covariance matrices corresponding to the model uncertainties are decreased at each time step by a factor $\gamma < 1$:

$$\mathbf{R}_{\mathrm{s}}(t) = \gamma \mathbf{R}_{\mathrm{s}}(t-1) \tag{49}$$

$$\mathbf{R}_{\mathrm{p}}(t) = \gamma \mathbf{R}_{\mathrm{p}}(t-1) \tag{50}$$

A further feature of the DEKF implemented here is the possibility of complete and partial switch off. For example, during vehicle stand-still, noise would be the only input to the DEKF; therefore, both state and parameter estimation schemes are switched off. Consequently, the DEKF is deactivated whenever zero velocity is approached.

Additionally, when the output signals corresponding to yaw rate, lateral acceleration and longitudinal velocity are below certain thresholds, implying that the signal information is less than the noise, then the parameter estimator is also switched off and the previous parameter estimates are maintained.

5. Results

The DEKF algorithm used here is implemented in the industry standard MATLAB® [24] functional programming environment.

Available data for a rearwheel drive executive saloon car was used to demonstrate the efficacy of the estimator. The data sets comprise the vehicle parameters and the dynamic vehicle states obtained both from an independent simulation using an alternative software package as well as actual measured data from a single test drive using an actual vehicle.

The alternative simulated data was generated by the simulation software-package ve-DYNA® [25]. The advantage of using simulated data, *e.g.* ve-DYNA, as a comparison is the possibility to obtain the non-measurable states for reference, as shown initially in ref. [26]. Figure 3 shows that the DEKF works well for state and parameter estimation for such simulated, noise-free data. Further results contained in this article confirm these preliminary findings and also show that the DEKF estimator is capable of handling realistic data from an actual test drive in the presence of measurement noise.

Data from the single test drive provides a realistic data set, *e.g.* with combined braking and cornering, as well as measurement noise, similar to that which can be expected in a practical application.

The example uses data that were obtained by driving on a public road at low speed. The manoeuvres carried out consisted of acceleration, braking and cornering. Data were measured over a time span of 135 s with a sampling period of 50 ms. Figure 4 shows the steer angle δ and the wheel velocities corresponding to the rotational velocities ω_{ij}, which were used as inputs for the DEKF. Figure 5 shows the reference outputs forward velocity v_x, yaw rate $\dot{\psi}$ and measured lateral acceleration $a_{y,\mathrm{sensor}}$.

Data for the tyres used on the vehicle – the parameters for the Magic Formula tyre model – were available. Parameters for slightly different tyres for the TMeasy tyre model were also available. This deliberate discrepancy provided the possibility to investigate the sensitivity of the DEKF to the tyre model, including the accuracy of such parameters. The estimator was then run with both tyre models. Figure 6 shows the estimated parameters: mass m, moment of inertia J_z and position b of the cog when using the tyre models, namely, Magic Formula and TMeasy. It can be seen that the Magic Formula tyre model provides final estimates within a range of about 4% of the actual values. However, with the same settings the use of the TMeasy

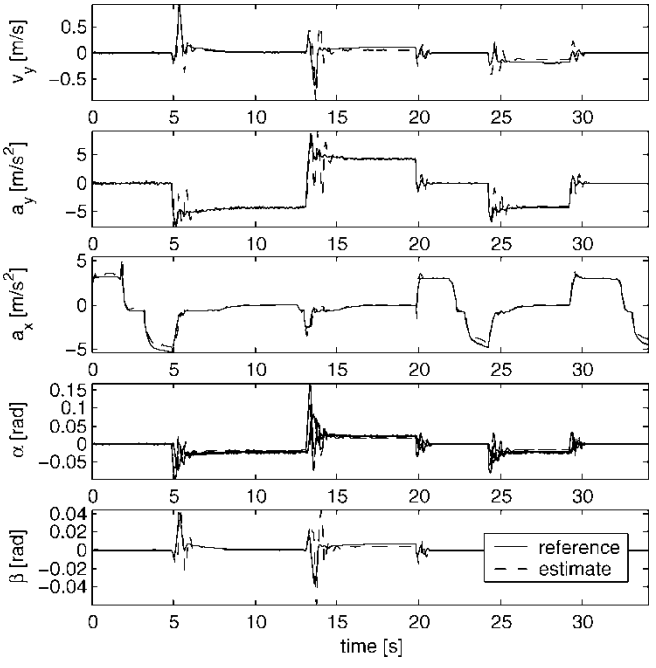

Figure 3. Estimated states for noise-free simulation data.

tyre model provides worse estimates, giving a final error in terms of the estimated mass of the order 20%.

The results for the state estimation using both the Magic Formula tyre model and the TMeasy tyre model are shown in figure 7, which depicts the estimates of the lateral velocity v_y, the lateral acceleration a_y, vehicle slip angle β and the front left wheel tyre slip angle α_{fl}, the vertical force $F_{z\mathrm{fl}}$ and the slip rate s_{fl}. The input data were also used within an independent

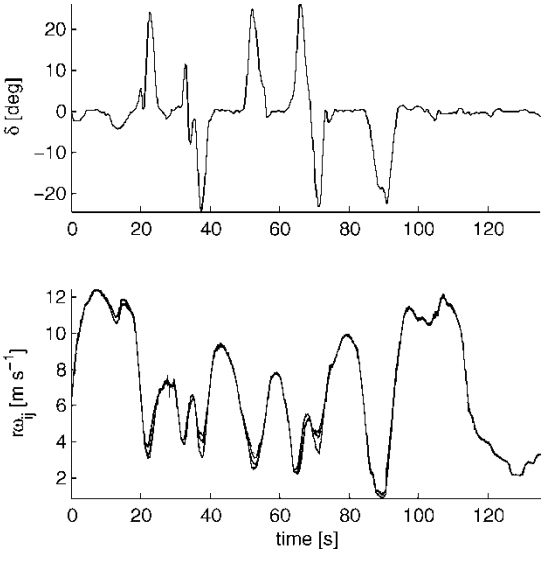

Figure 4. Input to DEKF.

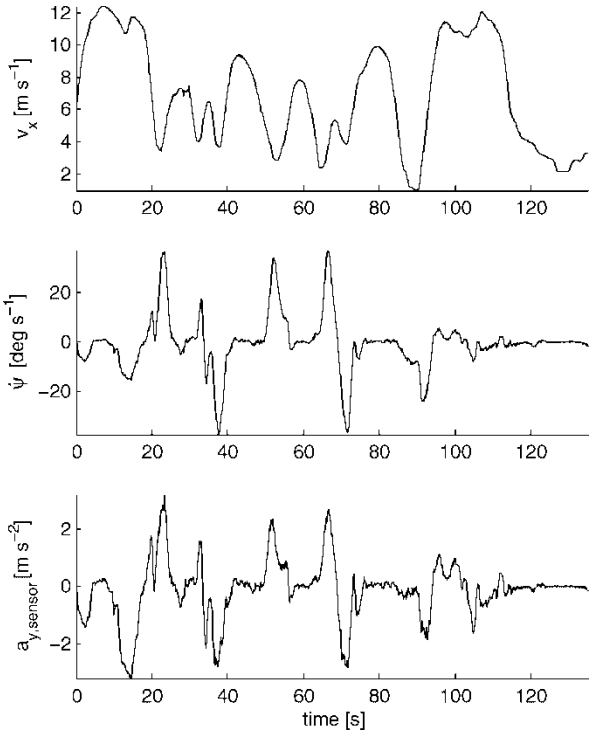

Figure 5. Reference outputs to DEKF.

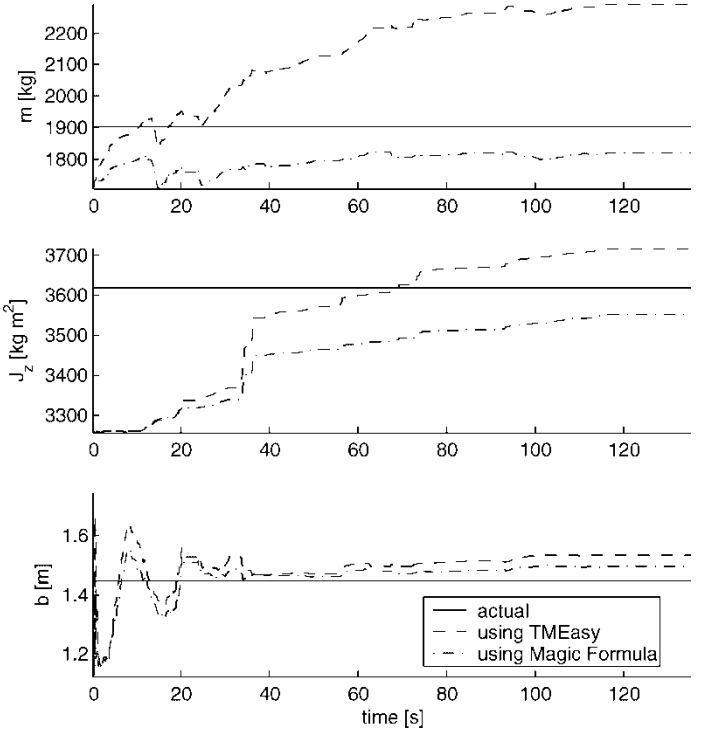

Figure 6. Estimated parameters mass m, moment of inertia J_z and longitudinal position b of the cog.

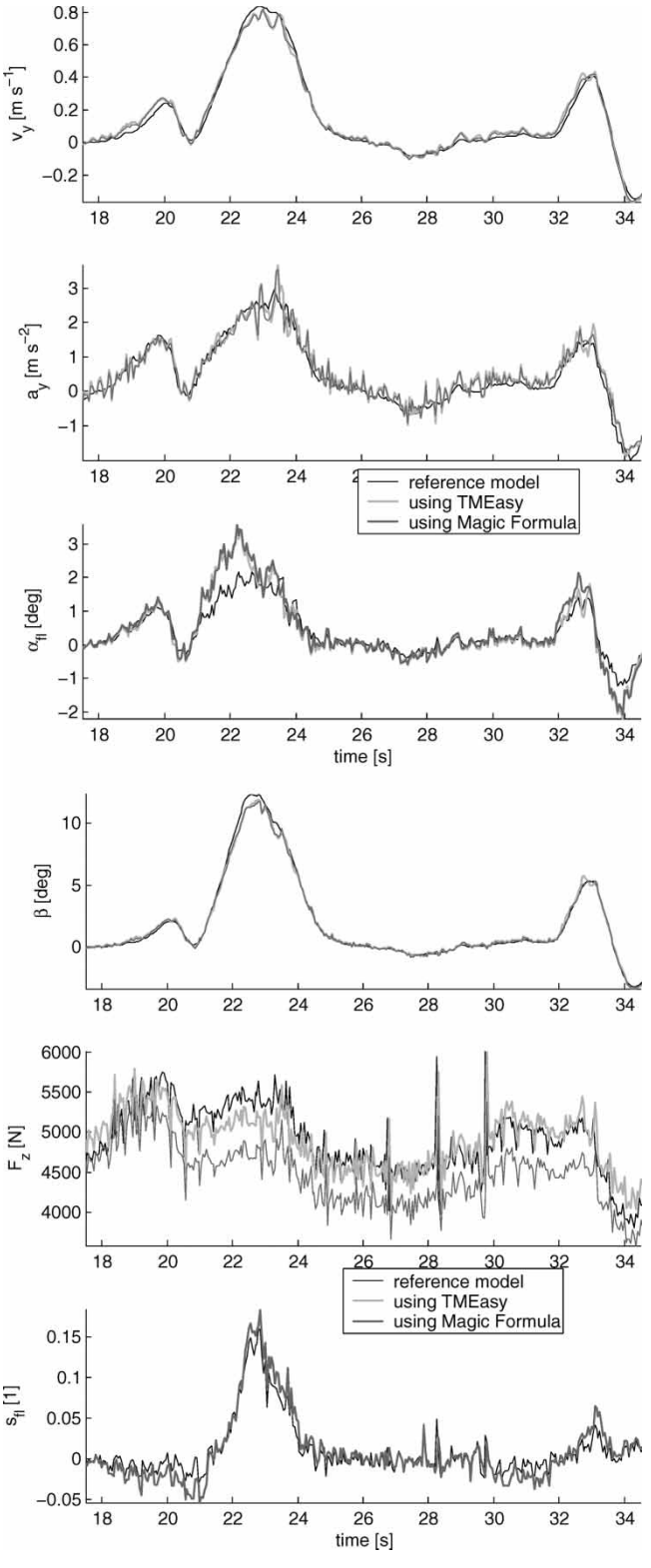

Figure 7. Estimated states.

Table 1. RMS error of selected states.

State	Using TMeasy	Using Magic Formula
v_y (m s^{-1})	0.027668	0.032576
a_y (m s^{-2})	0.23524	0.39377
β (rad)	0.013016	0.013524
α_{fl} (rad)	0.0070118	0.0081403
$F_{z\mathrm{fl}}$ (N)	547.77	407.18
s_{fl} (1)	0.014151	0.014447

reference vehicle simulation model to obtain reference values for the non-measurable states. Comparing the state estimates from the DEKF, using both tyre models with the reference simulation, it can be seen that the estimation is successful. By considering the root mean square error (RMS) of the estimates over a period of 135 s versus the reference simulation as given (see results given in table 1), it is found that the errors are acceptably small and appear to be independent of the tyre model used. Only the estimation of the vertical force differs appreciably from the reference data. This is believed to be caused by the strong dependence of the vertical forces on the vehicle mass, which, for the time range shown, has not converged sufficiently towards the actual values, but is known to differ by up to 8%. There appears to be interdependence between the error in the mass estimation and the error in the vertical force estimation. It can be seen that the DEKF is able to compensate for inaccurate vehicle and tyre parameters in the case of the state estimator, thus demonstrating that it is able to provide fairly good estimates for the main states.

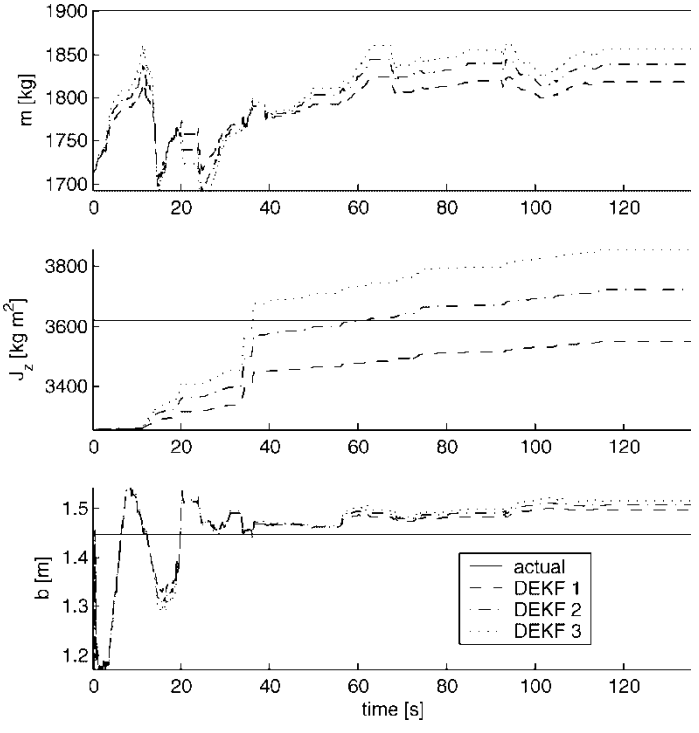

Figure 8. Estimated parameters mass m, moment of inertia J_z and longitudinal position b of the cog for various settings of the process noise covariance matrix $\mathbf{R}_{\mathrm{p}}$.

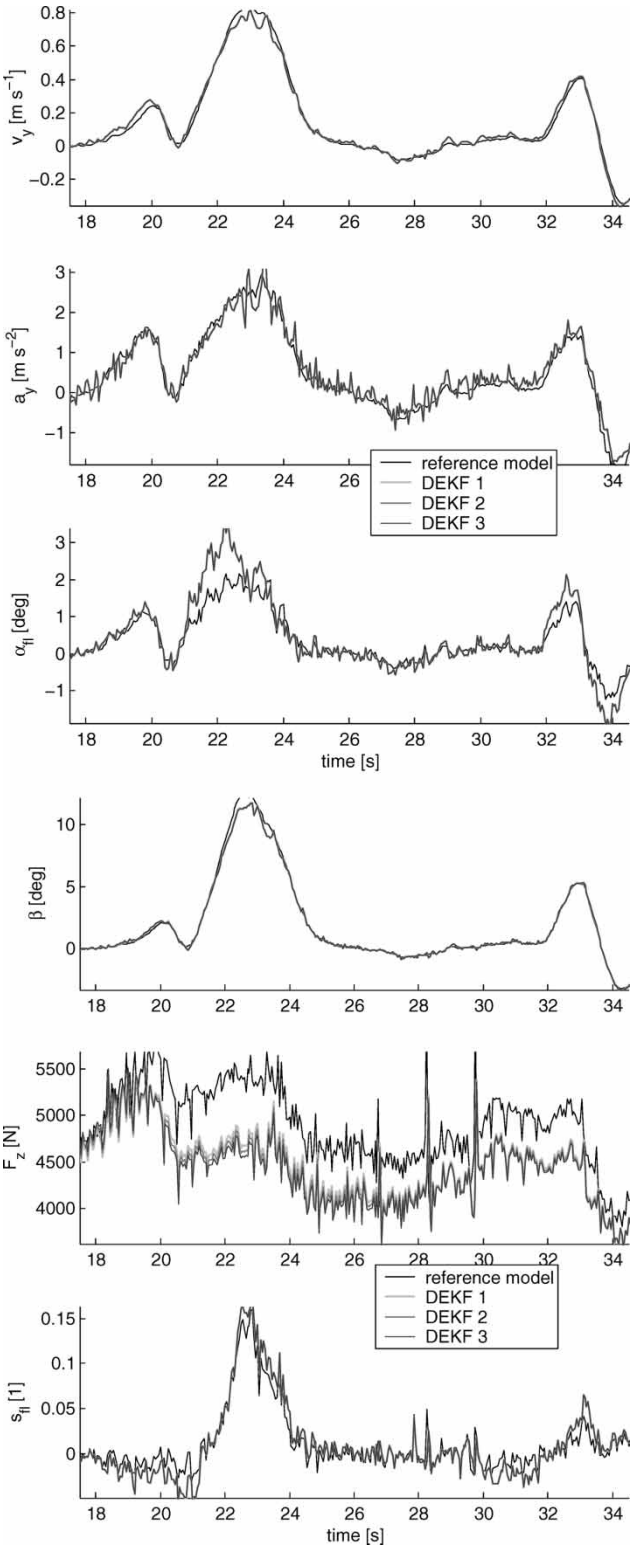

Figure 9. Estimated states for various settings of the process noise covariance matrix $\mathbf{R}_p$.

Table 2. Root squared error of selected states for various process noise covariance matrix $\mathbf{R}_p$.

State	DEKF1	DEKF2	DEKF3
v_y (m s^{-1})	0.032576	0.032012	0.031152
a_y (m s^{-2})	0.39377	0.37471	0.3481
β (rad)	0.013524	0.013451	0.01334
α_{fl} (rad)	0.0081403	0.0080705	0.0079272
F_{zfl} (N)	407.18	400.18	396.68
s_{fl} (1)	0.014447	0.014413	0.014356

In contrast, it is found that the parameter estimator is significantly more sensitive than the state estimator, both in terms of dependency on the accuracy of the vehicle and tyre models used and of the noise. From the results obtained, the importance of using the correct tyre data is clearly evident. Inaccurate coefficients for the tyre model result in large errors for the parameter estimation.

It is instructive to note the influence of the process noise covariance matrices on the DEKF. The results obtained when running the estimator three times, using the Magic Formula only, with initial process noise covariance matrix $\mathbf{R}_p$ given by equation (48) as well as $2\mathbf{R}_p$ or $3\mathbf{R}_p$, are stored in the data sets DEKF1, DEKF2 and DEKF3, respectively. Figure 8 shows the influence of the choice of $\mathbf{R}_p$ on the parameter estimation. However, the final estimates are still within a range of approximately $\pm 6\%$ for all three estimations.

Figure 9 shows that the state estimation is very similar for all three cases. The RMS error, given in table 2, shows again that the DEKF is capable of compensating for incorrect parameters. It can be concluded that the selection of the process noise covariance matrix is a significant factor for the parameter estimation.

6. Conclusions

This article has demonstrated the application of the DEKF technique for realising a model-based vehicle state and parameter estimator. This technique makes use of two parallel driven EKFs, which interact in a 'boot-strapping' way. Whilst one of the two EKFs is configured for the estimation of the main vehicle parameters, the other EKF is configured for estimating the vehicle states. One advantage of this technique is that with an efficient estimator and an improved accuracy of the parameter estimates, the model uncertainties within the state estimator decrease, thus allowing an enhancement of the quality of the state estimation. A further benefit is the possibility to switch off the parameter estimator, once the parameter estimates converge to satisfactory values or when the signal/noise ratio indicates disturbed input and output signals. In this case, constant parameter estimates are maintained, thus reducing the uncertainties for the state estimator.

The estimator is implemented in the Matlab/Simulink software environment and is based on a four-wheel dynamic vehicle model with different interchangeable tyre models. The latter feature offers the added flexibility to investigate the sensitivity of the estimator when using different tyre models.

Evaluation of the state and parameter estimator with both independently simulated data and measured data from a test drive using different tyre models shows that the state estimator is reasonably robust in terms of coping with variations in the tyre model. It is able to compensate for inaccuracies in the tyre parameters. However, the parameter estimator is much more sensitive both in terms of the tyre models and in terms of the initial settings of the KF

process noise covariance matrices. In general, the results to date are promising and show the effectiveness of this approach. The principle of replacing the existing individual state estimators, required by the various stability control systems within a vehicle, by one comprehensive single state and parameter estimator has been demonstrated, and potential benefits have been highlighted.

Further work is planned to extend the estimator by increasing the number of states and parameters, whilst at the same time improving stability and computational efficiency. Of particular interest is the inclusion of the vehicle's environment, such as the road friction μ, which could be treated as an additional state to be estimated.

References

[1] Bauer, H. (Ed.), 2000, *Automotive Handbook* (5th edn) (Robert Bosch GmbH: Stuttgart).

[2] Bolzern, P., Cheli, F., Falciola, G. and Resta, F., 1999, Estimation of the non-linear suspension tyre cornering forces from experimental road test data. *Vehicle System Dynamics*, **31**(1), 23–34. doi:10.1076/vesd.31.1.23.2100.

[3] Venhovens, P.J.T. and Naab, K., 1999, Vehicle dynamics estimation using Kalman filters. *Vehicle System Dynamics*, **32**(2–3), 171–184. doi:10.1076/vesd.32.2.171.2088.

[4] Zuurbier, J. and Bremmer, P., 2002, State estimation for integrated vehicle dynamics control. *Proceedings of the 6th International Symposium on Advanced Vehicle Control (AVEC)*, Hiroshima, Japan.

[5] Satria, M. and Best, M.C., 2002, Comparison between Kalman filter and robust filter for vehicle handling dynamics state estimation, *SAE 2002 World Congress*, Detroit, Michigan, 4–7 March, Warrendale: SAE Society of Automotive Engineers. SAE technical paper series 2002-01-1185.

[6] Huh, K., Kim, J. and Yi, K., 2003, Monitoring system design for estimating the lateral tyre force. *Proceedings of the Institution of Mechanical Engineers, Part D: Journal of Automobile Engineering*, **217**, 247–256. doi:10.1243/09544070360613219.

[7] Lingman, P. and Schmidtbauer, B., 2001, Road slope and vehicle mass estimation using Kalman filtering. *Proceedings of the 17th IAVSD Symposium in The Dynamics of Vehicles on Roads and on Tracks*, Lyngby, Denmark.

[8] Will, A.B. and Żak, S.H., 1997, Modelling and control of an automated vehicle. *Vehicle System Dynamics*, **27**, 131–155.

[9] Wong, J.Y., 2001, *Theory of Ground Vehicles* (3rd edn) (John Wiley & Sons, Inc.: New York).

[10] Kiencke, U. and Nielsen, L., 2000, *Automotive Control Systems* (Springer: Berlin).

[11] Chee, W., 2001, Measuring yaw rate with accelerometers. *Future Transportation Technology Conference*, Costa Mesa, California, SAE technical paper series 2001-01-2535.

[12] Stöcker, H. (Ed.), 1998, *Taschenbuch der Physik* (3rd edn) (Verlag Harri Deutsch: Thun und Frankfurt am Main).

[13] Pacejka, H.B. and Bakker, E., 1991, The magic formula tyre model. *Proceedings of the 1st International Colloquium on Tyre Models for Vehicle Dynamic Analysis* (Swets & Zeitlinger: Amsterdam), pp. 1–18.

[14] Fiala, E., 1954, Seitenkräfte am rollenden Luftreifen. *VDI Zeitschrift*, **96**(29), 973–979.

[15] Hirschberg, W., Rill, G. and Weinfurter, H., 2002, User-appropriate tyre-modelling for vehicle dynamics in standard and limit situations. *Vehicle System Dynamics*, **38**(2), 103–125. doi:10.1076/vesd.38.2.103.5620.

[16] Pacejka, H.B., 2002, *Tyre and Vehicle Dynamics* (Butterworth–Heinemann: Oxford).

[17] Lidner, L., 1991, Experience with the magic formula tyre model. *Proceedings of the 1st International Colloquium on Tyre Models for Vehicle Dynamic Analysis* (Swets & Zeitlinger: Amsterdam), pp. 30–46.

[18] Kalman, R.E., 1960, A new approach to linear filtering and prediction problems. *Transactions of the ASME–Journal of Basic Engineering, Series D*. **82**, 35–45.

[19] Young, P.C., 1974, Recursive approaches to time series analysis. *Bulletin of the Institute of Mathematics and its Applications*, **10**, 209–224.

[20] Wan, E.A. and Nelson, A.T., 2001, Dual extended Kalman filter methods. In: S. Haykin (Ed.) *Kalman Filtering and Neural Networks*, Chapter 5 (John Wiley & Sons: New York).

[21] Wan, E. and Nelson, A., 1997, Neural dual extended Kalman filtering: applications in speech enhancement and monaural blind signal separation. *Proceedings of Neural Networks for Signal Processing Workshop, IEEE.*

[22] Welch, G. and Bishop, G., 2002, *An Introduction to the Kalman Filter* (University of North Carolina: Chapel Hill).

[23] Sasiadek, J.Z. and Wang, Q., 2003, Low cost automation using INS/GPS data fusion for accurate positioning. *Robotica*, **21**, 255–260. doi:10.1017/S0263574702004757.

[24] The MathWorks, Inc., 2003, MATLAB. Available online at: http://www.mathworks.com. (accessed April 2003).

[25] TESIS, 2003, ve-DYNA, Gesellschaft für Technische Simulation und Software mbH. Available online at: http://www.tesis.de (accessed October 2003).

[26] Wenzel, T.A., Burnham, K.J., Blundell, M.V. and Williams, R.A., 2004, Approach to vehicle state and parameter estimation using extended Kalman filtering. *Proceedings of the 7th International Symposium on Advanced Vehicle Control AVEC04*, HAN University, Arnhem, NL, 23–27 August, pp. 725–730.

Nomenclature

a_x	longitudinal acceleration ($\mathrm{m\,s^{-2}}$)
a_y	lateral acceleration ($\mathrm{m\,s^{-2}}$)
$a_{y,\mathrm{sensor}}$	measured lateral acceleration ($\mathrm{m\,s^{-2}}$)
b	distance between cog and front axle (m)
b_a	distance between accelerometer and front axle (m)
c	distance between cog and rear axle (m)
f	state equations
F_{xij}	longitudinal forces on each wheel (N)
F_{yij}	lateral forces on each wheel (N)
F_{zij}	vertical forces on each wheel (N)
g	gravitational acceleration ($\mathrm{m\,s^{-2}}$)
h	height of cog (m)
h_s	height of cog of sprung mass (m)
h_z	height of accelerometer above roll axis (m)
h	output equations
$\mathbf{H}_\mathrm{s}$, $\mathbf{H}_\mathrm{p}$	Jacobian matrix of output for state/parameter estimator
i	front(f) or rear(r)
j	left(l) or right(r)
J_{sx}	moment of inertia of sprung mass around longitudinal axis ($\mathrm{kg\,m^2}$)
J_z	moment of inertia around vertical axis ($\mathrm{kg\,m^2}$)
$\mathbf{J}_\mathrm{s}$	Jacobian matrices for state estimates
$\mathbf{K}_\mathrm{s}$, $\mathbf{K}_\mathrm{p}$	Kalman gain matrices for state/parameter estimator
ℓ	length of wheel base ($\ell = b + c$) (m)
m	mass of vehicle (kg)
m_s	sprung mass (kg)
M_{zij}	self-aligning moment off each tyre (N m)
r	tyre radius (m)
$\mathbf{R}_\mathrm{s}$, $\mathbf{R}_\mathrm{p}$	process noise covariance matrices for state/parameter estimator
s_{ij}	wheel slip rate
t_f, t_r	front and rear track width (m)
$\mathbf{u}$	input vector
v_cog	velocity of the centre of gravity ($\mathrm{m\,s^{-1}}$)
v_{ij}	forward wheel speed ($\mathrm{m\,s^{-1}}$)
v_x	longitudinal velocity ($\mathrm{m\,s^{-1}}$)
v_y	lateral velocity ($\mathrm{m\,s^{-1}}$)
$\mathbf{v}$	output noise vector
$\mathbf{w}$	process noise vector
$\mathbf{x}_\mathrm{s}$, $\mathbf{x}_\mathrm{p}$	state/parameter vector
$\mathbf{y}$	output vector
α_{ij}	wheel slip angles (rad)
β	body side slip angle (rad)
β_ϕ	roll damping constant (Nm s)
γ	reduction factor for process noise covariance matrices

δ	steer angle (rad)
Γ	torque around z-axis (N m)
κ_ϕ	roll stiffness constant (N m)
$\boldsymbol{\sigma}_\mathrm{s}, \boldsymbol{\sigma}_\mathrm{p}$	measurement noise covariance matrices for state/parameter estimator
ϕ	body roll angle (rad)
$\boldsymbol{\Phi}_\mathrm{s}, \boldsymbol{\Phi}_\mathrm{p}$	estimate error covariance matrices for state/parameter estimator
$\dot{\psi}$	yaw rate (rad s^{-1})
ω_{ij}	wheel rotational velocity (rad s^{-1})